

Self-organization and Mechanical Properties of Active Filament Bundles

Karsten Kruse^{1, 2, 3, *} and Frank Jülicher^{1, 2, †}

¹*Max-Planck-Institut für Physik komplexer Systeme, Nöthnitzer Str. 38, 01187 Dresden, Germany*

²*Institut Curie, Physicochimie, UMR CNRS/IC 168, 26 rue d'Ulm, 75248 Paris Cedex 05, France*

³*Max-Planck-Institut für Strömungsforschung, Bunsenstr. 10, 37073 Göttingen, Germany*

(Dated: October 26, 2019)

A phenomenological description for active bundles of polar filaments is presented. The activity of the bundle results from crosslinks, that induce relative displacements between the aligned filaments. Our generic description is based on momentum conservation within the bundle. By specifying the internal forces, a simple minimal model for the bundle dynamics is obtained, capturing generic dynamic behaviors. In particular, contracted states as well as solitary and oscillatory waves appear through dynamic instabilities. The introduction of filament adhesion leads to self-organized persistent filament transport. Furthermore, calculating the tension, homogeneous bundles are shown to be able to actively contract and to perform work against external forces. Our description is motivated by dynamic phenomena in the cytoskeleton and could apply to stress-fibers and self-organization phenomena during cell-locomotion.

PACS numbers: 87.16.-b, 05.45.-a, 47.54.+r, 87.15.-v

I. INTRODUCTION

The cytoskeleton of eucaryotic cells is a complex three dimensional network of protein filaments, most prominently actin filaments and microtubules [1, 2]. Its elastic and viscous properties are essentially defining the mechanical or material properties of living cells. This network resembles in many aspects a polymer solution or a gel. The main difference from usual polymer materials is its intrinsic activity. In fact, the cytoskeleton is constantly remodeled through the polymerization and depolymerization of filaments, as well as through the formation and breakup of crosslinks. In addition, the crosslinks may be active, leading to further dynamics. All these activities are regulated by the cell which is thus able to direct intracellular transport, to separate its chromosomes and to cleave during cell division, to exert forces on the environment, or to move on a substrate. These processes rely on a number of enzymes interacting with actin filaments and microtubules [1, 2, 3].

The study of active polymer systems requires completely new tools and techniques as compared to the well developed analysis of equilibrium properties, that relies on powerful concepts of equilibrium statistical physics. Indeed, such systems are intrinsically far from equilibrium, and the dynamics at equilibrium, that is usually studied in polymer physics [4, 5, 6], is not sufficient for the description of active systems. On the contrary, experimental studies of the cytoskeleton under simplified conditions have revealed its ability to self-organize. Namely, the contraction of filament bundles [7], the formation of asters and vortices [8, 9, 10, 11], as well as the formation of networks [12] were found *in vitro*. Using a cell

extract, even the formation of bipolar spindles without microtubule organizing centers has been seen [13]. Cell fragments containing only the actin cytoskeleton, but neither the nucleus nor microtubules, can propagate on a substrate [14], where the locomoting state coexists with a stationary spherically symmetric state [15]. In a mixture of actin filaments and motors, active reptation in a polymer solution has been observed [16]. Let us finally mention, that experiments probing mechanical properties of living cells have revealed active responses of the cytoskeleton to external forces, see, e.g., Ref. [17].

First steps towards a theoretical understanding of active polymer systems have mostly aimed at describing pattern-formation. In one-dimensional filament bundles, polarity sorting [18], contraction [19, 20], and propagating waves [21] have been observed. Self-organization has also been seen to induce bending waves and complex motion in axonemes [22, 23]. In two dimensions, the effects of active crosslinks on spatially fixed but freely rotating filaments have been studied for a homogeneous [24] as well as for a dynamic motor distribution [25]. Furthermore, the viscoelastic response of solutions of semi-flexible polymers and active centers has been studied [26].

Motivated by the dynamics of the cytoskeleton, we discuss in this paper the generic behavior presented by bundles of aligned filaments in the presence of mobile crosslinks. To this end we develop a simple, yet general phenomenological description of active filament bundles, that emphasizes symmetries rather than any particular interaction mechanism. Like actin filaments and microtubules, which have two structurally different ends, the filaments are supposed to be polar. The crosslinks are mobile and considered to be formed by small aggregates of molecular motors [1, 2, 3, 27]. Hydrolyzing a chemical fuel, such a motor is able to exert forces on a filament. Motors cross-linking a pair of filaments may thus induce relative displacements between them. The direction of the force applied by a motor on a filament is uniquely

*karsten@mpipks-dresden.mpg.de

†julicher@mpipks-dresden.mpg.de

determined by the orientation of the filament [28]. In fixed aster-like structures of microtubules this leads to an accumulation or depletion of motors in the center of the aster [29].

Active filament bundles provide very simple examples of active filament networks and can be discussed by a one-dimensional description. Note, however, that in addition to their simplicity, such filament bundles actually occur in animal cells. They are, for example, part of stress fibers which generate contractile forces, and of the contractile ring in dividing cells [2]. *In vitro*, the contraction of actin bundles in the presence of myosin motors has been observed [7].

The phenomenological equations of motion for the filament densities, which we derive below, capture the general properties of the dynamics of active bundles on larger scales. As we will show, filament bundles can generate contractile tension and contractions. Furthermore, we find a scenario of dynamic instabilities between a homogeneous stationary state, and dynamic propagating and oscillating solutions. Some of these results have been published previously in Refs. [20, 21].

The outline of our manuscript is as follows. In section II, we derive phenomenological equations for an active filament bundle based on momentum balance. A simple minimal model which can be used to discuss many physical principles is studied systematically in Section III. In particular, we are interested in the behavior for large times, which is characterized by the attractors of the system. In Section IV we go beyond the minimal model and discuss briefly the effects of dynamic motor distributions. As we show in Section V, a bundle can generate motion with respect to a substrate if we take filament adhesion into account. The generation of tensile stresses in active bundles as well as the effects of forces applied at the bundle ends are the subject of Section VI. The paper concludes with a discussion of the results in Section VII.

II. PHENOMENOLOGICAL DESCRIPTION OF ACTIVE FILAMENT BUNDLES

We present a simple description for the dynamics of active filament bundles. The essential feature of motor-filament interactions is that the direction of the force applied by a motor on a filament is uniquely determined by the orientation of the filament [28]. Therefore, symmetry arguments are central in the development of our description.

A. Densities of filaments and motors

The bundle is characterized by the number densities of filaments and of motor complexes projected on the bundle axis, which leads to an effective one-dimensional description. Since filament bending and entanglements can be ignored in the bundle, we describe filaments as rigid rods. Filaments are aligned along the x -axis and we distinguish the two sub-populations of filaments with their plus-end pointing into the positive and negative x -direction, denoted plus and minus, respectively. These populations are described by the densities c^+ and c^- , such that, e.g., $c^+(x) dx$ gives the number of filaments with their plus-end in the positive x -direction and their center located in the interval $[x, x + dx]$. We assume, that motors are small compared to the filament length and will be treated as point-like in our description. The number density of motors is denoted by m .

The filament and motor densities satisfy the conservation laws

$$\partial_t c^+ = D \partial_x^2 c^+ - \partial_x J^+ \quad (1)$$

$$\partial_t c^- = D \partial_x^2 c^- - \partial_x J^- \quad (2)$$

$$\partial_t m = D_m \partial_x^2 m - \partial_x J \quad (3)$$

Here, D and D_m are effective diffusion constants of filaments and motors, respectively, while the currents J^\pm and J are generated by the active interaction between motors and filaments. As filaments do not flip, the number of filaments of either orientation is conserved.

B. Active filament currents and force

1. Momentum conservation

In the absence of external forces, the total momentum is conserved in the filament bundle. Forces acting within the bundle lead to an exchange of momentum with the environment or between filaments. Since filaments are treated as rigid, extended objects with momentum distributed along the full length of the filament, we introduce the momentum densities $\pi^\pm(x, y)$. These densities represent the momentum at position y carried by all plus- or minus-filaments, respectively, with their centers located at position x . The momentum balance can then be expressed as

$$\partial_t \pi^+(x, y) + \partial_y \sigma^+(x, y) - f_{\text{int}}^+(x, y) = f_{\text{fl}}^+(x, y) + f_{\text{m}}^+(x, y) + f_{\text{ext}}^+(x, y) \quad (4)$$

$$\partial_t \pi^-(x, y) + \partial_y \sigma^-(x, y) - f_{\text{int}}^-(x, y) = f_{\text{fl}}^-(x, y) + f_{\text{m}}^-(x, y) + f_{\text{ext}}^-(x, y) \quad (5)$$

Here, momentum flux along filaments centered at x is given by the tensions $\sigma^\pm(x, y)$. Momentum exchange

between filaments is nonlocal and described by the in-

ternal force densities $f_{\text{int}}^{\pm}(x, y)$, which include all active filament interactions via motors. The force densities $f_{\text{fl}}^{\pm}(x, y)$, $f_{\text{m}}^{\pm}(x, y)$, and $f_{\text{ext}}^{\pm}(x, y)$ are source and sink terms, describing momentum exchange with the environment. They result from friction with the fluid (f_{fl}), from motors moving along a single filament (f_{m}), and from external forces (f_{ext}). In all terms, x refers to filaments with center at position x , while y denotes a position in space, where a force is acting and momentum is exchanged. Momentum conservation in the absence of external forces requires, that

$$\int dx [f_{\text{int}}^+(x, y) + f_{\text{int}}^-(x, y)] = 0 \quad . \quad (6)$$

This implies, that any force generated by active crosslinks on a filament is balanced by an opposite force acting on other filaments, i.e., internal forces at a point y are balanced when integrated over all filaments. Therefore, total momentum $\Pi = \int dx dy (\pi^+ + \pi^-)$ only changes in the presence of external forces (ignoring boundary terms):

$$\frac{d}{dt} \Pi = \int dx dy [f_{\text{ext}}^+(x, y) + f_{\text{ext}}^-(x, y) + f_{\text{fl}}^+(x, y) + f_{\text{fl}}^-(x, y)] \quad (7)$$

Inertial terms are negligible in a slowly moving bundle, such that we can set $\partial_t \pi^{\pm} = 0$. Equations (4) and (5) then express a balance of forces.

In the most simple case where friction is local, we can write for the density of friction forces

$$f_{\text{fl}}^{\pm}(x, y) = \eta J^{\pm}(x) R(x - y) \quad (8)$$

Here, η is a friction coefficient per unit length and $R(x)$ is a function characterizing the distribution of energy dissipation along moving filaments. If all filaments are of the same length ℓ , a simple choice is $R(x) = 1$ for $|x| < \ell/2$ and $R(x) = 0$ otherwise. However, the function $R(x)$ can also account for situations with a distribution of filament lengths. Then, $R(x)$ is related to the probability, that a given filament is longer than $2|x|$.

The forces exerted by motors moving along a single filament are linear in the filament and motor densities,

$$f_{\text{m}}^{\pm}(x, y) = \eta_m \Gamma m(y) c^{\pm}(x) R(x - y) \quad , \quad (9)$$

where η_m is the friction coefficient corresponding to single motors and Γ a coefficient characterizing their binding to and motion on filaments.

2. Forces acting on filaments

While the internal forces are balanced at a point y when integrated over all filaments, the total force $\int dy f_{\text{int}}^{\pm}(x, y)$ acting on filaments centered at a given position x does not vanish in general. Integration of Eqs. (4) and (5) with respect to y reveals that this force is balanced by friction forces:

$$\eta \ell J^{\pm}(x) = \int dy [f_{\text{int}}^{\pm}(x, y) + f_{\text{m}}^{\pm}(x, y)] \quad (10)$$

where $\ell = \int dx R(x)$ is the average filament length. Since friction of motors is extremely small as compared to filament friction, $\eta_m \ll \eta \ell$, the contribution of f_{m}^{\pm} can be neglected under most circumstances, where $f_{\text{int}} \gg f_{\text{m}}$. In the following, we set $\eta_m = 0$.

In order to write explicit expressions for the currents, we need a model for the internal forces in the bundle. Let us consider the case when clusters of three or more cross-linked filaments form rarely enough, such that their contribution to the internal forces can be neglected. This holds, for example, in the case of a low motor density or for motors with a low duty ratio, which is the fraction of time a motor spends attached to a filament [30]. In the case when two-filament interactions dominate, we may split the internal forces into those between filaments of the same and those of opposite orientation. We write

$$f_{\text{int}}^+ = f_{\text{int}}^{++} + f_{\text{int}}^{+-} \quad (11)$$

and analogously for f_{int}^- . A motor may crosslink two filaments and thus exert forces of opposite sign on each of them, whenever they have an overlap. Assuming that the probability for two filaments to interact increases quadratically with filament density, we write

$$f_{\text{int}}^{\pm\pm}(x, y) = \int dz c^+(x) c^+(z) R(y - x) R(y - z) m(y) F_{\text{mot}}^{\pm\pm}(z - x, y - x) \quad (12)$$

Here, $F_{\text{mot}}^{\pm\pm}(\xi, \zeta)$ is the average force acting on plus-filaments at a distance ζ from the center exerted by motors, that cross-link with other plus-filaments located at a distance ξ from the first, see Fig. 1. The product

$R(y - x) R(y - z)$ gives the probability, that a filament at x has an overlap at y with a filament at z . Here, the position of a filament is given by the position of the filament's center. Analogous expressions hold for the in-

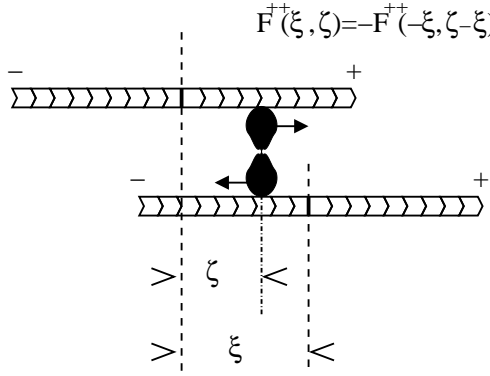


FIG. 1: Schematic representation of the forces exerted by an active crosslink on two plus-filaments. The filaments' centers are indicated by the dashed lines, whereas the dotted-dashed line marks the position of the active crosslink. The arrows indicate the direction of the forces applied on the filaments.

ternal forces between minus-filaments as well as between filaments of opposite orientation.

The forces $F_{\text{mot}}^{\pm\pm}$ and $F_{\text{mot}}^{\pm\mp}$ obey the following symmetry relations. *Actio* equals *reactio* demands that under an exchange of filaments, the force changes sign:

$$F_{\text{mot}}^{\pm\pm}(\xi, \zeta) = -F_{\text{mot}}^{\pm\pm}(-\xi, \zeta - \xi) \quad (13)$$

$$F_{\text{mot}}^{\pm\mp}(\xi, \zeta) = -F_{\text{mot}}^{\mp\pm}(-\xi, \zeta - \xi) \quad (14)$$

see Fig. 1. Using relation (12), the internal forces satisfying the above equations verify Eq. (6), which assures momentum conservation. Space inversion symmetry requires

$$F_{\text{mot}}^{++}(\xi, \zeta) = -F_{\text{mot}}^{--}(-\xi, -\zeta) \quad (15)$$

$$F_{\text{mot}}^{+-}(\xi, \zeta) = -F_{\text{mot}}^{-+}(-\xi, -\zeta) \quad (16)$$

3. A simple model

The forces $F_{\text{mot}}^{\pm\pm}$ as well as the dispersion R of the filament lengths can be chosen in various ways. The simple functional forms described below generate all classes of solutions that we have observed for different choices.

We choose

$$R(\zeta) = \begin{cases} 1 & \text{for } |\zeta| \leq \ell/2 \\ 0 & \text{for } |\zeta| > \ell/2 \end{cases} \quad (17)$$

corresponding to the case when all filaments are of the same length. The most simple choices of the motor forces obeying the symmetry relations are

$$F_{\text{mot}}^{\pm\pm}(\xi, \zeta) = A\eta\ell \text{sgn}(\xi) \quad (18)$$

$$F_{\text{mot}}^{\pm\mp}(\xi, \zeta) = \mp B\eta\ell, \quad (19)$$

where $\text{sgn}(\xi) = 1$ for $\xi > 0$ and -1 otherwise. Using

Eq. (10), this leads to the currents

$$J^{++}(x) = A \int_{-\ell}^{\ell} d\xi \text{sgn}(\xi) c^+(x + \xi) c^+(x) M(x, \xi) \quad (20)$$

$$J^{--}(x) = A \int_{-\ell}^{\ell} d\xi \text{sgn}(\xi) c^-(x + \xi) c^-(x) M(x, \xi) \quad (21)$$

$$J^{\pm\mp} = \mp B \int_{-\ell}^{\ell} d\xi c^{\mp}(x + \xi) c^{\pm}(x) M(x, \xi) \quad (22)$$

where

$$M(x, \xi) = \int d\zeta m(x + \zeta) R(\zeta) R(\zeta - \xi) \quad (23)$$

is the number of motors in the overlap of filaments at x and at $x + \xi$.

Our minimal model [20] is obtained by assuming a homogenous distribution of motors and by neglecting the dependence of the overlap on ξ . The currents then read

$$J^{\pm\pm}(x) = \alpha \int_0^{\ell} d\xi [c^{\pm}(x + \xi) - c^{\mp}(x - \xi)] c^{\pm}(x) \quad (24)$$

$$J^{\pm\mp}(x) = \mp \beta \int_{-\ell}^{\ell} d\xi c^{\mp}(x + \xi) c^{\pm}(x), \quad (25)$$

where α and β are the respective coupling constants for filaments of the same and opposite orientation.

C. Motor currents

The active, non-diffusive current of motors at a position y depends on all filaments that have an overlap with this point and can interact with motors there. The lowest order term for J reads

$$J(y) = \Gamma \int d\xi [c^+(y + \xi) - c^-(y + \xi)] m(y) R(\xi) \quad (26)$$

where Γ is a coefficient characterizing the speed of motors, see Eq. (9). The different signs of both terms take into account, that motors are transported long filaments according to their orientation.

When using the currents (20) to (22) we require, for consistency, $B\Gamma \geq 0$, ensuring that in all situations the direction of motion of a motor with respect to the filaments is the same.

III. THE MINIMAL MODEL

We discuss the properties and behaviors of the minimal model defined by Eqs. (1), (2), (24), and (25). To this end, it is convenient to use dimensionless coordinates and parameters. We define $x' = x/\ell$ and measure lengths in units of the filament length ℓ , and a dimensionless time variable $t' = tD/\ell^2$. Furthermore, we introduce dimensionless densities $c' = c\ell$ and use dimensionless coupling

constants $\alpha' = \alpha\ell/D$ and $\beta' = \beta\ell/D$. Suppressing the primes for simplicity, the minimal model is defined by

$$\begin{aligned} \partial_t c^+(x) &= \partial_x^2 c^+(x) - \alpha \partial_x \int_0^1 d\xi [c^+(x+\xi) - c^+(x-\xi)] c^+(x) \\ &\quad + \beta \partial_x \int_{-1}^1 d\xi c^-(x+\xi) c^+(x) \end{aligned} \quad (27)$$

$$\begin{aligned} \partial_t c^-(x) &= \partial_x^2 c^-(x) - \alpha \partial_x \int_0^1 d\xi [c^-(x+\xi) - c^-(x-\xi)] c^-(x) \\ &\quad - \beta \partial_x \int_{-1}^1 d\xi c^+(x+\xi) c^-(x) . \end{aligned} \quad (28)$$

It follows immediately from these equations, that the homogeneous state $c^\pm(x) = c_0^\pm = \text{const.}$ is a stationary solution for all values of the parameters.

A. Oriented bundles - Contraction

If all filaments are of the same orientation, one is left with a single equation

$$\partial_t c(x) = \partial_x^2 c(x) - \alpha \partial_x \int_0^1 d\xi [c(x+\xi) - c(x-\xi)] c(x) . \quad (29)$$

Here, c represents either c^+ or c^- , depending on the orientation of the filaments. This nonlinear integro-differential equation is the most simple description of the active dynamics of a filament bundle. Many of the basic physical principles underlying self-organization of filament bundles can already be discussed using this equation.

1. Linear stability analysis

Consider a system of length L with periodic boundary conditions and let us study the stability of the homogeneous state with respect to small perturbations. Periodic boundary conditions imply that the bundle forms a ring. In eucaryotic cells such rings appear, e.g., in the late stages of cell division. With these boundary conditions, the filament density is most conveniently represented by a Fourier expansion

$$c(x) = \sum_k c_k e^{ikx} , \quad (30)$$

with $k = 2\pi n/L$, $n = 0, \pm 1, \dots$ and where $c_{-k} = c_k^*$. Up to first order in the Fourier components c_k , the dynamics

the dynamic equations for the filament densities in dimensionless form

(29) reads

$$\frac{d}{dt} c_k = - (k^2 - 2\alpha c_0 (1 - \cos k)) c_k \quad (31)$$

$$\equiv \lambda(k) c_k , \quad (32)$$

for all k . This relation implies that for $\alpha c_0 \leq k^2/2(1 - \cos k)$ the mode c_k decays in time, because then $\lambda(k) \leq 0$. It follows that the most unstable mode is the one corresponding to the smallest non-zero wave number $k = 2\pi n/L$ with $n = 1$. This can be demonstrated using $(\frac{2\pi}{L})^2/2(1 - \cos \frac{2\pi}{L}) \leq (\frac{2\pi n}{L})^2/2(1 - \cos \frac{2\pi n}{L})$ for all $n > 1$ which can be verified by induction using the equivalent condition $n^2 - n^2 \cos(2\pi/L) - 1 + \cos(2\pi n/L) \geq 0$. Therefore, the homogeneous state is linearly stable as long as $\alpha \leq \alpha_c$, where the critical value α_c is determined by $\lambda(2\pi/L) = 0$. Explicitly,

$$\alpha_c = \frac{2\pi^2}{c_0 L^2 (1 - \cos(2\pi/L))} . \quad (33)$$

The critical value α_c is positive and decreases with increasing c_0 and L (for $L \geq 1$). Note, that for bundle sizes $L \geq 1$, we have $0 < \alpha_c < \infty$.

2. Contracted states

If the homogeneous state is unstable, the system evolves to an inhomogeneous steady state. We can calculate this state by numerically solving the dynamic equations or, in the vicinity of the bifurcation, using a systematic expansion in Fourier modes. To third order in c_1 the equation for the steady state $\partial_t c = 0$ reads

$$F(\alpha) c_1 - G(\alpha) |c_1|^2 c_1 = 0 , \quad (34)$$

with $F(\alpha) = \lambda(2\pi/L)$ and $G(\alpha)$ given by Eqs. (B6) and (B7), see Appendix B. Note, that $F(\alpha_c) = 0$. Expanding F and G at $\alpha = \alpha_c$, we find expressions for the Fourier amplitudes c_1 and c_2 , given by Eqs. (B8) and (B9). This

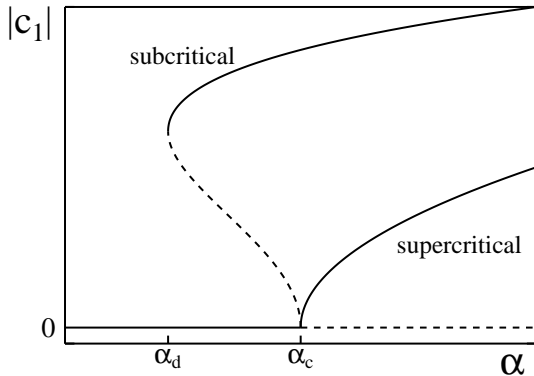


FIG. 2: Schematic representation of the modulus of the first spatial Fourier-component of stationary states as a function of α . Presented are both cases of a super- and of a subcritical bifurcation. Solid lines represent stable, dashed lines unstable solutions. In both cases, the homogeneous state is stable for $\alpha < \alpha_c$ and unstable otherwise. In the supercritical case, i.e., if $F/G > 0$ for $\alpha > \alpha_c$, the bifurcating solution exists for $\alpha > \alpha_c$ and is stable, while in the other case it exists for $\alpha < \alpha_c$ and is unstable. In the latter case, one usually finds stable stationary solutions coexisting with the stable homogeneous state in an interval $[\alpha_d, \alpha_c]$.

solution represents a localized distribution of filaments, i.e., a contracted bundle.

It follows from Eq. (34), that this contracted steady state exists if $F(\alpha)/G(\alpha) > 0$. Depending on whether the ratio F/G is positive for $\alpha > \alpha_c$ or for $\alpha < \alpha_c$, one distinguishes between super- and subcritical bifurcations, respectively, see Fig. 2. In the supercritical case, the contracted states obtained by solving Eq. (34) are stable. From Eq. (B8) one deduces that the bifurcation is supercritical for system sizes falling within particular intervals for which $4/(4n-1) < L < 4/(4n-3)$, $n = 1, 2, \dots$. In the subcritical case, these solutions are unstable. Still, stable solutions exist at the bifurcation. They appear before the critical point and coexist in some interval with the homogeneous state.

Figure 3 presents results of a numerical calculation, where the dynamical equations have been integrated using an Euler-algorithm with spatial discretiza-

tion $\Delta = 0.1$. Displayed is the modulus of the first Fourier-component $|c_1|$ of the attractors as a function of α for a system of length $L = 10$. The region of coexistence extends from $\alpha = \alpha_d$ up to α_c , where the homogeneous state becomes unstable.

For large α we find numerically, that transient states consisting of several contracted packets can occur, which however decay for long times to a steady state with one maximum. Their lifetime increases with increasing α .

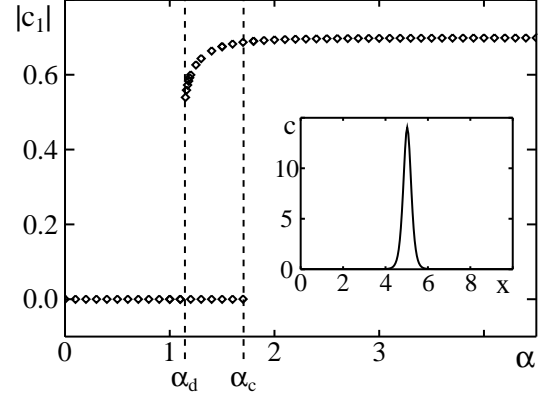


FIG. 3: The modulus of the first Fourier-component of stable stationary solutions of the minimal model as a function of α for $c_0 = 0.7$ and $L = 10$. The inset presents the non-homogeneous stationary solution for $\alpha = 1.5$. The scenario shown corresponds to a subcritical bifurcation, see Fig. 2.

3. Contraction dynamics

The contraction of the bundle is conveniently measured by the variance of the filament distribution

$$\sigma^2 = \frac{1}{N} \int_{-\infty}^{\infty} dx x^2 c(x) \quad , \quad (35)$$

where $N = \int_{-\infty}^{\infty} dx c(x)$ is the total number of filaments. Since the center of mass of the distribution is immobile due to momentum conservation, we have assumed without restriction of generality, that $\langle x \rangle = \int_{-\infty}^{\infty} dx x c(x) = 0$. The variance changes in time as

$$\begin{aligned} \frac{d}{dt} \sigma^2 &= \frac{1}{N} \int_{-\infty}^{\infty} dx x^2 \partial_t c(x, t) \\ &= \frac{2}{N} \int_{-\infty}^{\infty} dx c(x, t) + \frac{2}{N} \int_0^1 d\xi \left[\int_{-\infty}^{\infty} dx x c(x + \xi) c(x) - \int_{-\infty}^{\infty} dx x c(x - \xi) c(x) \right] \\ &= 2 - \frac{2}{N} \alpha \int_0^1 d\xi \xi \int_{-\infty}^{\infty} dx c(x + \xi) c(x) \quad . \end{aligned} \quad (36)$$

where we have used Eq. (29). The final expression reveals two opposing effects. The positive constant describes the

spreading of the bundle due to diffusion while the second

term takes into account the effect of the active interaction. Since its sign is negative the interaction between parallel filaments tends to contract the bundle. Note, that distributions for which $d\sigma^2/dt = 0$ do not necessarily correspond to stationary solutions of the dynamics (29).

B. Bundles of mixed orientation - Solitary waves

1. Linear stability analysis

In the general case, the linearization of Eqs. (27) and (28) around the homogeneous state $c^\pm(x) = c_0^\pm = \text{const}$ reads in Fourier-representation

$$\frac{d}{dt} \begin{pmatrix} c_k^+ \\ c_k^- \end{pmatrix} = \begin{pmatrix} \Lambda^{++} & \Lambda^{+-} \\ \Lambda^{-+} & \Lambda^{--} \end{pmatrix} \begin{pmatrix} c_k^+ \\ c_k^- \end{pmatrix}, \quad (37)$$

where the elements of the matrix $\Lambda(k)$ are given by

$$\begin{aligned} \Lambda^{\pm\pm}(k) &= -k^2 - 2\alpha(\cos(k) - 1)c_0^\pm \pm 2i\beta k c_0^\mp \\ \Lambda^{\pm\mp}(k) &= \mp 2i\beta \sin(k)c_0^\pm. \end{aligned} \quad (38)$$

For a system of length L with periodic boundary conditions, the wave numbers are $k = 2\pi n/L$ with $n = 0, 1, \dots$. In presence of the coupling between the filaments of opposite orientation, the matrix Λ is not diagonal. In order to assess the stability of the modes we have to determine the larger of the real parts $\lambda(k)$ of the complex eigenvectors of this matrix. Explicit expressions for these eigenvalues as well as for $\lambda(k)$ are given in App. A.

Numerically, we find again the mode with the smallest wave number $k = 2\pi/L$ to become unstable first. Also, the relation $\lambda(2\pi/L) = 0$ determines again a unique critical value α_c with the homogeneous state being linearly stable for $\alpha < \alpha_c$. Furthermore, $\alpha_c \geq 0$, independently of the values of the other parameters, see App. A. Hence, a sufficiently strong interaction between parallel filaments leads to an instability of the homogeneous state.

The critical value of α is a function of the remaining parameters

$$\alpha_c \equiv \frac{1}{c} g \left(\beta, \frac{\delta c}{c}, L \right), \quad (39)$$

where $c = c_0^+ + c_0^-$, $\delta c = c_0^+ - c_0^-$, and g is a dimensionless scaling function. In some limiting cases, explicit expressions for α_c can be obtained. For example, for $\delta c = 0$ one finds $g = 4\pi^2/L^2[1 - \cos(2\pi/L)]$ and in the limit $L \rightarrow \infty$ $g = 1$ if $\beta \neq 0$, whereas $g = 2/(1 + |\delta c|/c)$ for $\beta = 0$, see Eq. (33). These expressions reflect some general properties of α_c , namely it decreases monotonically with $|\delta c|/c$, L , and $|\beta|$ [20]. In particular, the decrease of α_c for increasing $|\delta c|$ is consistent with the finding, that interacting parallel filaments render the homogeneous state unstable.

2. Solitary waves

For $\beta \neq 0$, the eigenvalues of $\Lambda(k)$ are complex and the homogeneous state loses stability through a Hopf-bifurcation, leading to solutions that oscillate in time. Numerically, we find that at the bifurcation a solitary wave occurs of the form $c^\pm(x, t) = u^\pm(x - vt)$. This implies that at the bifurcation point time-translation invariance is broken while the invariance with respect to spatial translations remains intact. For small interaction strengths between filaments of opposite orientation, i.e., $|\beta| \ll 1$, solitary waves can be understood as a contracted distribution of filaments of one orientation, that is set into motion through the interaction with filaments of opposite orientation, which are homogeneously distributed, if both distributions are stable for $\beta = 0$.

In agreement with this picture, the solitary waves found numerically exhibit a well-pronounced maximum in the distribution of one kind of filaments, while the other distribution is comparatively flat. This holds also for solitary waves existing for large values of $|\beta|$. The above picture can be translated into a systematic procedure for determining solitary waves: writing $c^\pm(x, t) = u^\pm(x - vt)$, we can expand $u^\pm(x)$ in powers of β . For $\beta = 0$, we start from steady states as discussed above, which we denote as $c^\pm(x, t) = u_0^\pm(x)$. Solitary wave solutions are obtained by assuming that, e.g., u_0^+ is a contracted steady state, while u_0^- is homogeneous.

We can now write the *ansatz*

$$u^\pm(x) = u_0^\pm(x) + u_1^\pm(x)\beta + u_2^\pm\beta^2 + \dots \quad (40)$$

$$v = v_1\beta + v_3\beta^3 + \dots \quad (41)$$

The even terms in the expansion for v vanish by symmetry. Indeed, if $u^\pm(x - vt)$ is a solution for a given β , then $u^\pm(-x + vt)$ corresponds to $-\beta$, implying $v(\beta) = -v(-\beta)$. In each order β , we find a linear equation for u_k^\pm and v_k . Solving these equations in lowest order, we obtain

$$v_1 = 2c_0^- \quad (42)$$

$$u_1^+ = 0 \quad (43)$$

$$u_{1,k}^- = -\frac{2i \sin k c_0^- u_{0,k}^+}{k^2 - 2\alpha(1 - \cos k)c_0^-} \quad \text{for } k \neq 0. \quad (44)$$

This result is in good agreement with numerical solutions of Eqs. (27) and (28), see Ref. [21] and Fig. 4, where the velocity of a solitary wave is shown as a function of β . It increases monotonically and saturates for large β . While the saturated velocity depends on α , the initial slope $\lim_{\beta \rightarrow 0} \partial v / \partial \beta$ is independent thereof, as Eq. (42) indicates.

For any β , solitary wave solutions can be obtained near the instability via a systematic expansion in Fourier modes by using a solitary wave as *ansatz*, see App. B 2. There, it is furthermore shown, that for α close to α_c and small $|\beta|$ the expansion of the solitary wave in terms of Fourier-components, Eqs. (B11)-(B14), and the expansion in β , Eqs. (40) and (41), yield the same results.

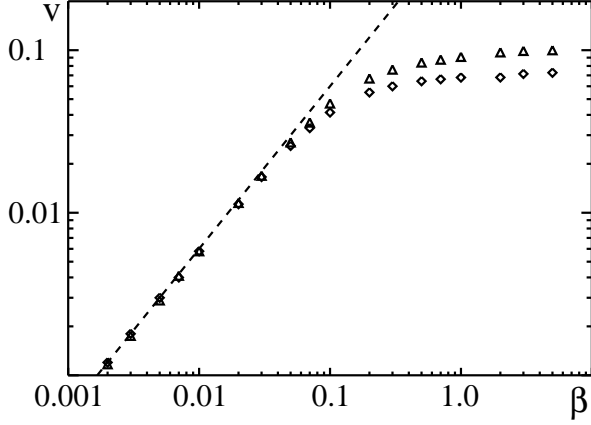


FIG. 4: The velocity of solitary wave solutions of the minimal model as a function of β for $\alpha = 1.2$ (triangles) and 2 (diamonds). The remaining parameters are $c_0^+ = 0.7$, $c_0^- = 0.3$, and $L = 10$. The dashed line represents the velocity as obtained from the perturbation calculation Eq. (42).

3. Phase diagram

Consider stable contracted distributions for both filament populations, c^+ and c^- , and $\beta = 0$. Changing β to a small non-zero value, which corresponds to switching on the interaction between filaments of opposite orientation, then sets both distributions into motion, although in opposite directions. The resulting spatio-temporal pattern is an oscillating wave, which consists of two oscillating distributions, that periodically penetrate each other. During an encounter they flatten and regain their original shape afterwards. An example of such an asymptotic solution is shown in Fig. 5. As in this example the numbers of filaments of each orientation are very different from each other one still gets the impression of an advancing distribution.

Based on the results for oriented bundles, we can thus sketch the phase-diagram for mixed bundles in the case $|\beta| \ll 1$. For system sizes $L > 4$, the bifurcations of the homogenous states are subcritical for $\beta = 0$. The corresponding critical values are denoted by $\alpha_{c,0}^\pm$, while for $\alpha > \alpha_{c,0}^\pm$ stable contracted distributions of the respective populations of plus- and minus-filaments exist. Assuming without loss of generality $\alpha_{d,0}^+ < \alpha_{c,0}^-$, contracted distributions of plus-filaments coexist with stable homogeneous distributions of minus-filaments in the interval $[\alpha_{d,0}^+, \alpha_{c,0}^-]$. As shown above, for $|\beta| \ll 1$, this leads to a corresponding region of solitary waves. For $\alpha > \max(\alpha_{d,0}^+, \alpha_{d,0}^-)$ a region of oscillatory waves exists, resulting from the interaction of contracted distributions of both, plus- and minus-filaments.

The bottom panels of Fig. 6 give a schematic representation of these findings. We use the time-averaged sum of the modules of the first spatial Fourier components of both distributions, $\langle |c_1^+| + |c_1^-| \rangle$, in order to charac-

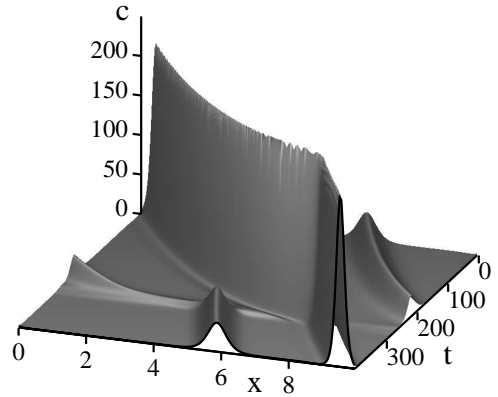


FIG. 5: An oscillating propagating wave solution of the minimal model for $\alpha = 2.5$, $\beta = 1.$, $c_0^+ = 0.7$, $c_0^- = 0.3$, and $L = 10$.

terize the state of the system. This value is displayed as a function of α for two different ratios of numbers of plus- and minus-filaments. In the first case, we find an interval of values for α , where the homogeneous state H and a solitary wave S_1 coexist, and an interval, where S_1 and an oscillatory wave O coexist. In the second case, also coexistence between two solitary waves S_1 and S_2 moving in opposite directions occurs. The direction of motion is thus an intrinsic property of the solution, not determined by global system parameters. The sketch also shows unstable invariant solutions.

The same figure also presents numerically obtained phase-diagrams for three different values of β and two different filament concentrations. For the lowest value of β it follows closely the picture given in the two bottom panels. Increasing β , we numerically did not find any other asymptotic behavior than presented so far. However, the α -intervals for which they exist, depend on β . In particular, for $c_0^+ = 0.55$ and $c_0^- = 0.45$, one solitary wave solution vanishes altogether as $|\beta|$ exceeds some critical value. Furthermore, the bifurcation through which the solitary waves lose stability changes from sub- to supercritical at $\beta \approx 0.01$.

For system sizes $1 < L < 4$ all bifurcations are supercritical and no coexistence can be observed. Otherwise, the global picture remains unchanged.

4. Oscillation and contraction

The existence of propagating solutions depends on the imposed boundary conditions. Imposing no-flux boundary conditions on a system of finite size, suppresses propagating solutions for long times. In general, the interaction between antiparallel filaments now tends to separate the two filament populations. Indeed, for $\beta > 0$, this interaction leads to a transport of plus-filaments to

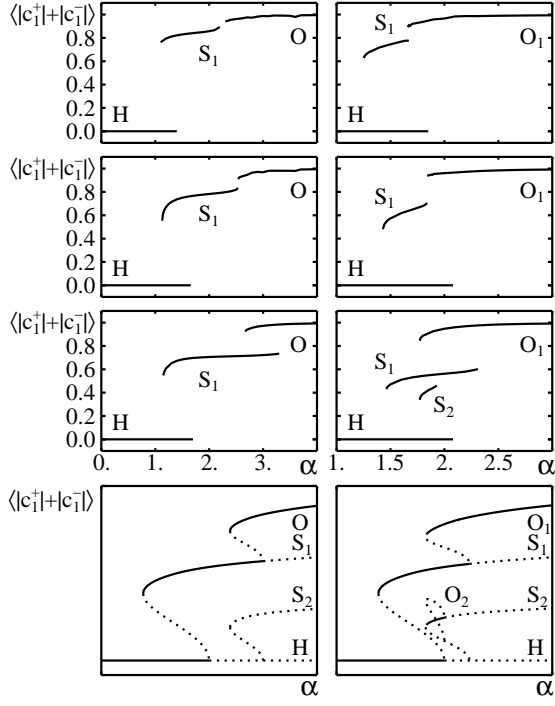


FIG. 6: The attractors of the minimal model represented by the time-averaged modulus of the first spatial Fourier-component as a function of α . The homogenous state is indicated by H, solitary waves by S, and oscillatory waves by O. The lowest panels give a schematic representation for $|\beta| \ll 1$ based on the phase diagram for $\beta = 0$ as explained in the text. Here, dashed lines indicate unstable solutions. The upper panels have been obtained by numerical integration of the minimal model, where from top to bottom $\beta = 0.1, 0.01$, and 0.001 , respectively. Left panels are for $c_0^+ = 0.7$ and $c_0^- = 0.3$, while right panels are for $c_0^+ = 0.55$ and $c_0^- = 0.45$. In all cases $L = 10$.

the left and of minus-filaments to the right. The system will thus end up in a steady non-homogeneous state, in which plus-filaments are mostly to the right of minus-filaments. Simultaneously, the system contracts if α is large enough. The Hopf-bifurcation in the case of periodic boundary conditions indicates, that contraction is accompanied by transient wave-like propagating modes. In this case, interesting asymptotic behavior is observed if polymerization and depolymerization of filaments is taken into account.

IV. DYNAMIC MOTOR DISTRIBUTIONS

We will now discuss briefly, how the bundle dynamics is influenced by dynamic, non-homogeneous motor distributions. The following discussion does not contain a systematic and exhaustive treatment of these systems, but rather highlights differences with respect to the minimal model described above. The main results are, that oriented bundles can exhibit solitary waves and that the

critical wave-number of the unstable mode can be finite. Furthermore, the homogeneous state can become unstable even if the interaction between filaments of the same orientation is absent. It may in some cases be re-stabilized by increasing the corresponding coupling constant A .

A. Dynamical equations

In order to study the effect of a dynamic motor distribution, we will use the motor forces given in Eqs. (18) and (19). For convenience we gather all the equations and write the full model. Again we will use dimensionless densities $c^\pm = c^\pm \ell$ and $m' = m/m_0$, where $m_0 = \frac{1}{L} \int_0^L dx m(x)$ and L is the system size. Furthermore, we use dimensionless space and time coordinates, $x' = x/\ell$ and $t' = tD/\ell^2$, as well as dimensionless parameters $A' = A m_0 \ell^2 / D$, $B' = B m_0 \ell^2 / D$, $\Gamma' = \Gamma \ell / D$, and $D'_m = D_m / D$. Suppressing the primes we thus have

$$\partial_t c^\pm = \partial_x^2 c^\pm - \partial_x J^{\pm\pm} - \partial_x J^{\pm\mp} \quad (45)$$

$$\partial_t m = D_m \partial_x^2 m - \partial_x J^{\mp\mp} \quad (46)$$

with

$$J^{\pm\pm}(x) = A \int_{-1}^1 d\xi \operatorname{sgn}(\xi) M(x, \xi) c^\pm(x + \xi) c^\pm(x) \quad (47)$$

$$J^{\pm\mp}(x) = \mp B \int_{-1}^1 d\xi M(x, \xi) c^\mp(x + \xi) c^\pm(x) \quad (48)$$

$$J(x) = \Gamma \int_{-\frac{1}{2}}^{\frac{1}{2}} d\xi [c^+(x + \xi) - c^-(x + \xi)] m(x) \quad (49)$$

where $M(x, \xi) = \int_{x - \frac{1}{2} + \xi}^{x + \frac{1}{2}} d\zeta m(\zeta)$ for $\xi > 0$ and $M(x, \xi) = \int_{x - \frac{1}{2}}^{x + \frac{1}{2} + \xi} d\zeta m(\zeta)$ for $\xi < 0$, see Eq. (23).

B. Oriented bundles

If only filaments of one orientation are present, then the dynamical equations simplify as in the case of the minimal model. Let c denote the distribution of filaments and consider a system of length L with periodic boundary conditions. The linearization of the time-evolution operator with respect to the homogeneous state $c(x) = c_0$ and $m(x) = m_0 = 1$ is in Fourier representation given by

$$\begin{pmatrix} -k^2 + 2A(1 - \frac{\sin k}{k})c_0 & -2A(\cos \frac{k}{2} - \frac{2}{k} \sin \frac{k}{2})c_0^2 \\ -2i\Gamma \sin \frac{k}{2} & -D_m k^2 - i\Gamma k c_0 \end{pmatrix}, \quad (50)$$

where $k = 2\pi n/L$, with $n = 0, 1, \dots$. For $\Gamma/D_m \rightarrow 0$, leading to a homogeneous motor distribution, the larger of the real parts of the two eigenvalues is $-k^2 + 2A(1 - \frac{\sin k}{k})c_0$. For $k \rightarrow 0$ it thus approaches the corresponding value in the minimal model, see Eq. (31).

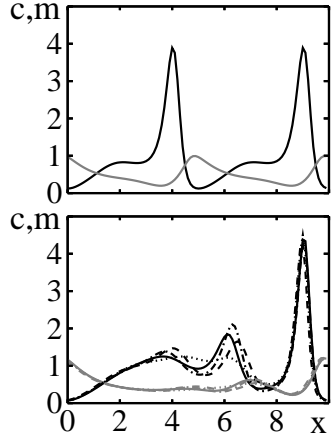


FIG. 7: Examples of attractors of the system with dynamic motor distribution in the case of filaments of one orientation only. The upper panel shows a solitary wave with a spatial period of half the system size, the lower panel an oscillatory wave. The black lines represent the filament distributions, the grey lines the motor distributions. In the lower panel, distributions at four different times are shown with different line styles and the highest maxima of the filament distribution have been superposed. Interestingly, both attractors coexist. The parameters are $\alpha = 1.5$, $\gamma = 1.5$, $D_m = 1.$, $c_0 = 1.$, $m_0 = 0.5$, and $L = 10$.

In contrast to the analogous situation in the minimal model, the eigenvalues of (50) are complex as long as $\Gamma \neq 0$. The homogeneous state thus loses stability through a Hopf-bifurcation, where the mode losing its stability first may now correspond to $k \neq 2\pi/L$. In addition, the number of asymptotic solutions is now larger: there are solitary waves with one as well as with several maxima, see Fig. 7 top. Furthermore, oscillatory waves have been found. In Fig. 7 bottom, such a solution is presented for several different times. As in the example shown, the oscillatory solutions may coexist with solitary wave solutions.

C. Bundles of mixed orientation

1. Linear stability analysis

In the general case, the linearization around the homogeneous state of the dynamics (45)-(49) reads in Fourier representation

$$\frac{d}{dt} \begin{pmatrix} c_k^+ \\ c_k^- \\ m_k \end{pmatrix} = \begin{pmatrix} \Lambda^{++} & \Lambda^{+-} & \Lambda^{+m} \\ \Lambda^{-+} & \Lambda^{--} & \Lambda^{-m} \\ \Lambda^{m+} & \Lambda^{m-} & \Lambda^{mm} \end{pmatrix} \begin{pmatrix} c_k^+ \\ c_k^- \\ m_k \end{pmatrix}, \quad (51)$$

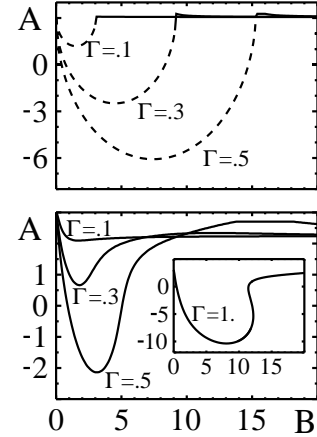


FIG. 8: Regions of stability of the homogenous state in the (A, B) -plane for the system with dynamic motor distribution, where the homogeneous state is stable below the lines shown. The upper panel is for the symmetric case $c_0^+ = c_0^- = 1.$, the lower panel for $c_0^+ = 1.$ and $c_0^- = 0.5$. In both cases, $L = 10$ and $D_m = 1.$. Solid lines indicate Hopf-bifurcations, dashed lines pitchfork bifurcations. The inset presents a case where increasing A can re-stabilize the homogeneous state.

where the elements of the matrix $\Lambda(k)$ are

$$\begin{aligned} \Lambda^{\pm\pm}(k) &= -k^2 + 2A(1 - \frac{\sin k}{k})c_0^\pm \pm iBk c_0^\mp \\ \Lambda^{\pm\mp}(k) &= \pm 2iB \frac{1 - \cos k}{k} c_0^\pm \\ \Lambda^{\pm m}(k) &= -2A(\cos \frac{k}{2} - \frac{2}{k} \sin \frac{k}{2})c_0^\pm \pm 2iB \sin \frac{k}{2} c_0^+ c_0^- \\ \Lambda^{m\pm}(k) &= \mp 2i\Gamma \sin \frac{k}{2} \\ \Lambda^{mm}(k) &= -D_m k^2 - i\Gamma k(c_0^+ - c_0^-) \end{aligned}$$

In contrast to the minimal model, the line in the (A, B) -plane limiting the region of stability of the homogeneous state depends non-monotonically on B . For large enough Γ it may even fold back on itself, such that increasing A may re-stabilize the homogeneous state. See Fig. 8, where this line is shown for different values of Γ and different filament concentrations. Note, that it may lie below $A = 0$. For the corresponding values of B no interaction between parallel filaments is thus necessary in order to produce an instability of the homogeneous state. The dependence of this border on Γ is also non-monotonous. In difference to the minimal model, the mode losing stability first may correspond to $k \neq 2\pi/L$.

For $c_0^+ \neq c_0^-$ the homogeneous state loses its stability always through a Hopf-bifurcation. In the symmetric case $c_0^+ = c_0^-$, this is true only for certain values of B , see Fig. 8. As A or B are increased, a second instability is encountered, when the stationary states transform into oscillatory states.

2. Asymptotic behavior

We find again three types of asymptotic behaviors: homogeneous states, solitary waves, and oscillatory waves. In contrast to the minimal model, solitary waves can exist even in the absence of interactions between filaments of opposite orientation, i.e., for $B = 0$. Note, that in this case the two filament densities do not decouple. Notably, by increasing Γ the direction of motion of solitary waves can be inverted.

V. FILAMENT-ADHESION

We now consider the case of a bundle, where filaments can adhere to a substrate. For simplicity, filament adhesion will be discussed in the framework of the minimal model.

Plus- and minus-filaments attached to the substrate are described by the densities a^+ and a^- , respectively. Free filaments attach to the substrate with rate Ω_a and attached filaments detach with rate Ω_d irrespective of their orientation. Attached filaments are assumed to be immobile, while they contribute to the motion of free filaments in the same way as these. Thus, generalizing Eqs. (27) and using dimensionless variables as introduced in Section III with $\omega_{a,d} = D\Omega_{a,d}/\ell^2$, the dynamic equations take the form

$$\partial_t c^+ = \partial_x^2 c^+ - \partial_x J^{++} - \partial_x J^{+-} - \omega_a c^+ + \omega_d a^+ \quad (52)$$

$$\partial_t c^- = \partial_x^2 c^- - \partial_x J^{--} - \partial_x J^{-+} - \omega_a c^- + \omega_d a^- \quad (53)$$

$$\partial_t a^+ = \omega_a c^+ - \omega_d a^+ \quad (54)$$

$$\partial_t a^- = \omega_a c^- - \omega_d a^- \quad (55)$$

with

$$J^{\pm\pm} = \int_0^1 d\xi [\alpha c^\pm(x + \xi) + \alpha' a^\pm(x + \xi) - \alpha c^\pm(x - \xi) - \alpha' a^\pm(x - \xi)] c^\pm(x) \quad (56)$$

and

$$J^{\pm\mp} = \mp \int_{-1}^1 d\xi [\beta c^\mp(x + \xi) + \beta' a^\mp(x + \xi)] c^\pm(x) \quad . \quad (57)$$

From now on, we consider the case $\omega_d > 0$ and assume periodic boundary conditions.

For all values of the parameters, the homogeneous state $c^\pm(x) = c_0^\pm = \text{const}$ and $a^\pm(x) = \omega_a c_0^\pm / \omega_d = \text{const}$ is stationary. It becomes unstable at a critical value α_c . For oriented bundles, the critical value is given by

$$\alpha_c = \alpha_{c,\text{mm}} \frac{\omega_a + \omega_d}{\mu \omega_a + \omega_d}, \quad (58)$$

where $\alpha_{c,\text{mm}}$ is the critical value for the minimal model, i.e., for $\omega_a = 0$, and $\mu = \alpha'/\alpha$. For $\beta \neq 0$ the bifurcation is of the Hopf-kind and the dependence of α_c on ω_a is shown in Fig. 9 for $\alpha' = 2\alpha$. For low values of $|\beta|$, adhesion tends to decrease the value of α_c , i.e., to destabilize the homogeneous state. For larger $|\beta|$ adhesion can both, stabilize and destabilize the homogeneous state, depending on the attachment rate ω_a . In the limit of large attachment rates, $\alpha_c < \alpha_{c,\text{mm}}$ and, i.e., large adhesion rates destabilize the homogeneous state.

Let us now analyze the attractors. In the case $\beta = 0$, the stationary distributions are readily obtained from those without adhesion. Indeed, if $c^\pm(x; 0)$ are the stationary distributions for $\omega_a = 0$, then $c^\pm(x; \omega_a) = \frac{\omega_d}{\mu \omega_a + \omega_d} c^\pm(x; 0)$ and $a^\pm(x; \omega_a) = \frac{\omega_a}{\mu \omega_a + \omega_d} c^\pm(x; 0)$. In the case $\beta \neq 0$ no such simple relations hold. However, in the limit of small attachment rates, i.e., $\omega_a \ll \omega_d$, solutions

can be obtained by expanding around solitary waves for $\omega_a = 0$. Let $c^\pm(x, t) = u_0^\pm(x - v_0 t)$ and $a^\pm(x, t) = 0$ be a solitary wave solution in the case $\omega_a = 0$. Assuming that for finite ω_a solutions of the form $c^\pm(x, t) = u^\pm(x - vt)$ and $a^\pm(x, t) = r^\pm(x - vt)$ exist, we write

$$v = v_0 + \omega_a v_1 + \dots \quad (59)$$

$$u^\pm = u_0^\pm + \omega_a u_1^\pm + \dots \quad (60)$$

$$r^\pm = \omega_a r_1^\pm + \dots \quad (61)$$

This expansion yields for every n linear equations for u_n^\pm and r_n^\pm . Here, the equations for r_n^\pm only depend on u_{n-1}^\pm and v_{n-1} . The equations for r_1^\pm can be solved explicitly. We find

$$r_1^\pm(x) = \frac{1}{e^{\omega_a T} - 1} \int_0^T dt' e^{\omega_a t'} u_0^\pm(x - v_0 t') \quad , \quad (62)$$

where $T = v_0 L$. This equation shows, that through the immobilization of filaments by adhesion, the system acquires a memory.

This result can in turn be used to calculate in first order in ω_a the total net current I associated with these solitary waves. Indeed, in lowest order this current is given by

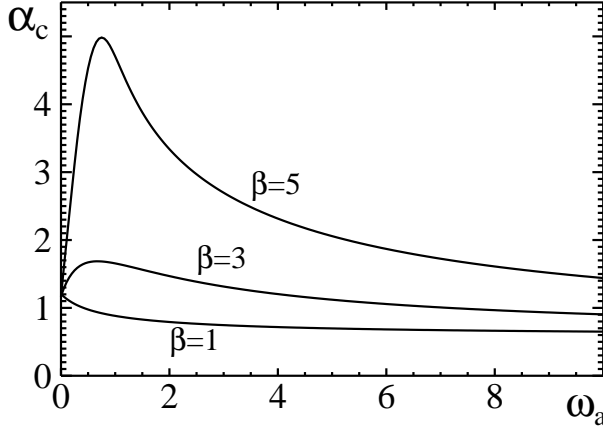


FIG. 9: The critical value of the minimal model including adhesion as a function of the adhesion rate ω_a for $c_0^+ = .7$, $c_0^- = .3$, $\alpha' = 2\alpha$, $\beta' = 2\beta$, $\omega_d = 1.$, and $L = 10$.

$$I = 2\omega_a \int_0^L dx \left\{ \alpha \int_0^1 d\xi \left[(r_1^+(x+\xi) - r_1^-(x-\xi)) u_0^+(x) + (r_1^-(x+\xi) - r_1^+(x-\xi)) u_0^-(x) \right] \right. \\ \left. + \beta \int_{-1}^1 d\xi \left[r_1^+(x+\xi) u_0^-(x) - r_1^-(x+\xi) u_0^+(x) \right] \right\} , \quad (63)$$

where, for simplicity, we have chosen $\alpha' = 2\alpha$ and $\beta' = 2\beta$. All other terms cancel each other. Evaluating this expression for r_1^\pm as given by (62) and with $u_0^\pm(x) = \sum_{n=-\infty}^{\infty} u_{0,n}^\pm e^{i2\pi nx/L}$ we obtain

$$I = 8\omega_a L^3 v_0 \alpha \sum_{n=1}^{\infty} A_n (|u_{0,n}^+|^2 + |u_{0,n}^-|^2) + O(\omega_a^2) , \quad (64)$$

where

$$A_n = \frac{\cos \frac{2\pi n}{L} - 1}{\omega_d^2 L^2 + 4\pi^2 n^2 v_0^2} \quad (65)$$

with v_0 and u_0^\pm depending on β as described in Sec. III B 2. This result shows, that through the adhesion of filaments to a substrate, solitary waves are accompanied with a net filament transport. Since $A_n < 0$ for all n , this transport occurs into the opposite direction as the motion of the wave. Remarkably, as indicated by the prefactor α , it is the interaction between *parallel* filaments that generates the current. Note, however, that for $\beta = 0$ we have $v_0 = 0$ and thus $I = 0$. Numerical results for I as a function of ω_a are shown in Fig. 10. For the dependence of I on the parameters α and β see Ref. [21].

VI. CONTRACTILE TENSION AND EXTERNAL FORCES

The tension $\Sigma(y)$ at any point y within the bundle is obtained by integrating the contributions of all filaments, i.e.,

$$\Sigma(y) = \int dx [\sigma^+(x, y) + \sigma^-(x, y)] , \quad (66)$$

where $\sigma^\pm(x, y)$ has been introduced in Eqs. (4) and (5). Taking into account momentum conservation, Eq. (6), one finds in the absence of external forces

$$\frac{d}{dy} \Sigma(y) = \int dx [f_{\text{fl}}^+ + f_{\text{fl}}^- + f_{\text{m}}^+ + f_{\text{m}}^-] . \quad (67)$$

This equation allows to calculate the tension profile by means of Eq. (8) if the currents J^\pm and the dispersion of filament lengths R are known.

Let us again assume $f_{\text{m}} \ll f_{\text{fl}}$ and distinguish between the contribution to the tension by the interactions between filaments of the same orientation, Σ_{\Rightarrow} , and by those between filaments of opposite orientation, Σ_{\Leftarrow} . The total tension in the bundle then is

$$\Sigma(y) = \Sigma_{\Rightarrow}(y) + \Sigma_{\Leftarrow}(y) . \quad (68)$$

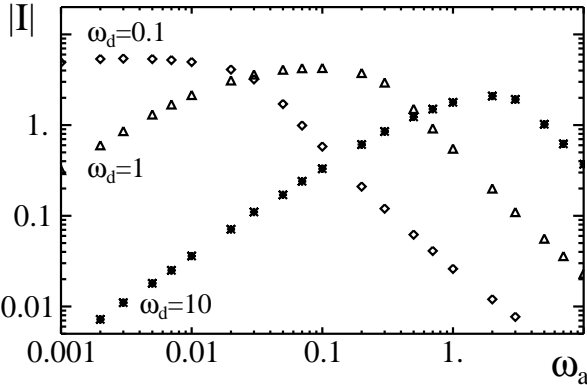


FIG. 10: The absolute value of the current as a function of the adhesion rate ω_a for $\alpha = 1.5$, $\beta = 2.$, $c_0^+ = 0.7$, $c_0^- = 0.3$, $L = 10$, and three different values of ω_d . Filaments are transported into the opposite direction the distribution moves to. Note, that the maximal current decreases and is reached at larger ratios of ω_a/ω_d as ω_d is increased.

From Eq. (67) we obtain

$$\Sigma_{\Rightarrow}(y) = -\eta \int dx (J^{++}(x) + J^{--}(x))Q(x-y) + \Sigma_{\Rightarrow}^{(0)} \quad (69)$$

$$\Sigma_{\Leftarrow}(y) = -\eta \int dx (J^{+-}(x) + J^{-+}(x))Q(x-y) + \Sigma_{\Leftarrow}^{(0)} \quad (70)$$

where $\frac{d}{dx}Q(x) = R(x)$ with $Q(0) = 0$, and $\Sigma_{\Rightarrow}^{(0)}$ and $\Sigma_{\Leftarrow}^{(0)}$ are constants of integration. As $Q(x)$ is non-zero for all $x \neq 0$, the tension at position y along the bundle seems to depend on the global state of the bundle. However, tension is a local quantity, which depends on the filament distributions only within an interval with a size of the order of the filament length. Introducing $P(x, \xi) = Q(x + \xi) - Q(x)$, we can rewrite the above expressions in an explicitly local form. For the minimal model we obtain

$$\begin{aligned} \Sigma_{\Rightarrow}(y) &= \frac{1}{2}\alpha\eta \int_{-\ell}^{\ell} d\xi \int dx c^+(x + \xi)c^+(x)P(x-y, \xi)\text{sgn}(\xi) \\ &\quad + \frac{1}{2}\alpha\eta \int_{-\ell}^{\ell} d\xi \int dx c^-(x + \xi)c^-(x)P(x-y, \xi)\text{sgn}(\xi) \end{aligned} \quad (71)$$

and

$$\begin{aligned} \Sigma_{\Leftarrow}(y) &= \frac{1}{2}\beta\eta \int_{-\ell}^{\ell} d\xi \int dx c^-(x + \xi)c^+(x)P(x-y, \xi) \\ &\quad - \frac{1}{2}\beta\eta \int_{-\ell}^{\ell} d\xi \int dx c^+(x + \xi)c^-(x)P(x-y, \xi) \end{aligned} \quad (72)$$

In contrast to the non-local function Q , P is a local function with $P(x, \xi) = 0$ for $|x| > 2\ell$. In writing the above equations, we have dropped constant contributions to the tension arising from the boundaries. Indeed, if we consider a situation with periodic boundary conditions, such boundary terms must vanish. We determine the integration constants $\Sigma_{\Rightarrow}^{(0)}$ and $\Sigma_{\Leftarrow}^{(0)}$ in such a way, that in the final expressions (71) and (72) constant contributions to the tension are absent.

The tension in the homogeneous state $c^\pm(x) = c_0^\pm$, is thus given by

$$\Sigma = \frac{1}{2}\eta\ell^3\alpha(c_0^+{}^2 + c_0^-{}^2) \quad . \quad (73)$$

In this case only the interaction between parallel filaments contributes to the active part of the bundle tension. For an oriented bundle, the tension is positive, i.e., contractile, whenever $\alpha > 0$.

More compact expressions can be obtained by the approximation $P(x, \xi) = \xi$ for $|x| < \ell/2$ and $P(x, \xi) = 0$ elsewhere. Then

$$\Sigma_{\Rightarrow}(y) \approx \frac{1}{2} \alpha \eta \int_{y-\ell/2}^{y+\ell/2} dx \int_{-\ell}^{\ell} d\xi |\xi| (c^+(x+\xi)c^+(x) + c^-(x+\xi)c^-(x)) \quad (74)$$

and

$$\Sigma_{\Leftarrow}(y) \approx \frac{1}{2} \beta \eta \int_{y-\ell/2}^{y+\ell/2} dx \int_{-\ell}^{\ell} d\xi \xi (c^+(x+\xi)c^-(x) - c^-(x+\xi)c^+(x)) . \quad (75)$$

For filament distributions that vary weakly over a filament length, this result corresponds to the expressions given in Ref. [20], with $\bar{\eta} = \eta/2$ and $\tilde{\eta} = \eta/4$.

Contractile tension in the bundle can give rise to contractile forces exerted by the bundle. In order to illustrate this, consider a homogeneous oriented bundle with constant filament density $c(x) = c_0$ inside a box $0 \leq x \leq L$ of size L while $c(x) = 0$ elsewhere. In order to stabilize this state, we impose boundary conditions which immobilize filaments within the intervals $[0, \ell]$ and $[L-\ell, L]$ near the ends. Such boundary conditions could be realized by attaching the filaments near the end to a substrate. This filament distribution is stationary and stable for $\alpha < \alpha_c$. We can calculate the force required to maintain the filaments near the ends immobile. The force density acting on immobile filaments with center at $x \in [0, \ell]$ is $f_{\text{ext}}(x) = \alpha \eta \ell c_0^2 (\ell - x)$ and analogously for attached filaments at the other end of the bundle. The total force acting on the ends is thus $F = \int_0^\ell f_{\text{ext}}(x) dx = \Sigma$. This result indicates, that the generated force is independent of the bundle length and increases with the filament density.

VII. DISCUSSION

In this work we have developed a physical description for the dynamics and mechanics of active filament bundles. In our one-dimensional description, we study the dynamics of the filament densities projected on an axis which is parallel to the filaments. The activity in these bundles results from active crosslinks, that create force dipoles between the filaments. Our derivation of the filament dynamics is based on momentum conservation within the bundle and its exchange via external forces. We have considered the most simple situation, where filament motion results from interactions of filament pairs. Taking the finite filament length into account leads to nonlocal momentum exchange in the bundle. On a formal level, this generated integrals in the dynamic equations. Alternatively, the bundle dynamics on scales much larger than the filament length could be described in a continuum limit, leading to non-linear partial differential equations [31]. However, the present approach offers a well-defined way to express the dynamics on all scales including the effect of filament overlap on filament sliding,

and can describe force balances and momentum flux in the bundle. This allows us to discuss bundle mechanics. Furthermore, the present approach stabilizes the dynamics on small scales and permits a straightforward numerical implementation.

Our analysis focussed on the minimal model, which permitted to discuss analytically and numerically the general types of behaviors of this class of systems. This model respects the underlying symmetries and generates generic dynamic behaviors. Starting with the homogeneous state, stable localized states and solitary waves can be generated through dynamic instabilities. A subsequent instability of solitary waves can then lead to oscillatory waves. All these bifurcations can be either subcritical or supercritical, depending on parameters, in particular, on the ratio of the filament length to the system size. Subcritical bifurcations imply, that several of these states can coexist for certain parameter values. Notably, solitary waves, propagating in opposite directions, can coexist. If filaments adhere to a substrate, similar patterns still exist. However, momentum is in this case no longer conserved and the corresponding propagating states show net filament transport.

Calculating the momentum flux along filaments in the bundle, we have obtained expressions for the bundle tension. We have shown, that interactions between filaments of the same orientation give rise to tension and bundle contraction. In particular, these interactions generate tension in the steady state of a stable homogeneous bundle.

It might seem odd at first glance that interactions between filaments of the same orientation are important. As in this case motors advance on both filaments approximately with the same speed, no relative motion is expected and one might wonder, what is the microscopic origin of these interactions. In general, interactions between filaments of the same orientation are induced by motors that do not move with the same speed on two cross-linked filaments. The most striking case is when a motor arrives on one filament at the end towards which it moves. Then, the motor stops at this end while continuing for a while to move on the second filament. Clearly, this induces relative filament sliding. Some evidence for this effect in mixtures of microtubules and associated motors has been presented in [13]. There are several other possible mechanisms which lead to motion with differ-

ent speeds along two displaced filaments. The motor speed can be affected by crowding of many motors on the filament. Such crowding would typically lead to a slowing down of motors as they approach the filament end [32]. Finally, there could be specific proteins bound to the filaments which affect the action of motors. If such proteins are distributed inhomogeneously along the filaments, they would induce strong interaction terms between filaments of the same orientation.

While in our minimal model the interactions between filaments of the same orientation are crucial for contraction and the occurrence of dynamical instabilities, we have shown that as soon as the dynamics and inhomogeneities of the motor distribution are taken into account, these behaviors already occur, if only filaments of opposite orientation interact. The full phase diagram is in this case considerably richer than for the minimal model, however, the same types of solutions persist. The main difference with respect to the minimal model is, that an oriented bundle will lose its stability through a Hopf bifurcation and generates a solitary wave.

Our equations describe the average behavior of the bundle and ignore fluctuations. However, numerical simulations of more macroscopic models show, that the phenomena described above persist qualitatively in the presence of fluctuations [20]. A thorough analysis of the effect of fluctuations will be the subject of a separate publication.

The general behaviors found in our models can describe observations in simplified experimental situations. In particular, the contraction, polarity sorting, and the evolution of the motor density in disordered bundles of actin filaments in the presence of ATP has been observed *in vitro* [7]. Our findings agree qualitatively with the observed behavior, however, more controlled and quantitative experiments are required for a more careful comparison. We hope that our work will stimulate new experiments *in vitro* on active behaviors of motors and filaments.

Our results could also apply to stress fibers. These are contractile actin bundles in cells lacking the obvious periodic organization of muscles [1]. As we have seen, in

such disordered structures, the generation of tension and contraction is possible through the interaction of filament pairs without the need of a muscle-like sarcomere structure. The periodic boundary conditions which we use in several examples correspond to the situation, where the bundle forms a ring and could apply for example to contractile rings which cleaves a cell during cell division.

Interestingly, the types of dynamic behaviors which we observe also include the phenomenology presented by fragments of fish keratocytes [14, 15]. These fragments consist of the lamellipodium, which is the flattened leading margin of these cells, responsible for their migration. Notably, they do contain neither the nucleus nor microtubules. These fragments exist in a symmetric stationary state as well as in an asymmetric locomoting state, where one can change between these states through sufficiently strong external perturbations [15]. Even though the active bundles studied in the present work are far from giving a description of moving keratocyte fragments, our results clearly indicate, that viewing the cytoskeleton as a dynamical system is important for understanding such phenomena. Our description of active bundles provides a firm basis for the development of more profound theories of active filament systems, which could help understanding self-organization and dynamic behaviors in living cells such as cell locomotion. Moving on into this direction will require a number of important additional ingredients. A three dimensional description should, for example, incorporate effects, such as the polymerization and depolymerization of filaments, non-mobile cross-linkers, and capping proteins.

APPENDIX A: EIGENVALUES OF THE LINEARIZED TIME-EVOLUTION OPERATOR

In the following we give the complete eigenvalues of the linearized time-evolution operator $\Lambda(k)$ of the minimal model and show, that $\alpha_c > 0$.

The eigenvalues of $\Lambda(k)$, Eq. (30) are

$$\begin{aligned} \lambda^\pm &= -k^2 + \alpha(1 - \cos k)c - 2i\beta k\delta c \\ &\pm \left\{ \alpha^2(1 - \cos k)^2\delta c^2 - \beta^2 k^2 c^2 + \beta^2 \sin^2 k(c^2 - \delta c^2) + 2i\alpha\beta k(1 - \cos k)c\delta c \right\}^{1/2} . \end{aligned} \quad (\text{A1})$$

In this expression $c = c_0^+ + c_0^-$ and $\delta c = c_0^+ - c_0^-$. The real part of λ^+ , which determines the stability of the homogeneous state against small perturbations, is thus

$$\lambda(k) = -k^2 + \alpha(1 - \cos k)c + \left\{ \frac{1}{2} \sqrt{a^2 + b^2} + \frac{1}{2}a \right\}^{1/2} \quad (\text{A2})$$

with

$$\begin{aligned} a &= \alpha^2(1 - \cos k)^2\delta c^2 - \beta^2 k^2 c^2 + \beta^2 \sin^2 k(c^2 - \delta c^2) \\ b &= 2\alpha\beta k(1 - \cos k)c\delta c . \end{aligned} \quad (\text{A4})$$

For $\alpha = 0$ this implies

$$\lambda(k) = -k^2 + \frac{1}{2}|a| + \frac{1}{2}a = -k^2 \quad (\text{A5})$$

because in this case

$$a = -\beta^2(k^2c^2 - \sin^2 kc^2 + \sin^2 k\delta c^2) < 0. \quad (\text{A6})$$

Furthermore, the derivative of λ with respect to α is of the form

$$\frac{\partial \lambda}{\partial \alpha} = A_0 + A_1\alpha + A_2\alpha^3 \quad (\text{A7})$$

with $A_i > 0$, $i = 0, 1, 2$. Together with $\lim_{\alpha \rightarrow -\infty} \lambda(\alpha) < 0$, Eqs. (A5) and (A7) imply that there is a unique critical value $\alpha_c > 0$, determined by $\lambda(k = 2\pi/L; \alpha = \alpha_c) = 0$, such that the homogenous state is linearly stable unless $\alpha > \alpha_c$.

APPENDIX B: NON-HOMOGENEOUS ATTRACTORS CLOSE TO α_c

We calculate the attractors of the minimal model close to the critical value α_c by keeping the leading nonlinear

terms in the Fourier-representation and show, that for $|\beta| \ll 1$ the result is equivalent to the one obtained in Sec. III B 2 through the expansion in β .

1. Oriented bundles

In Fourier-representation the stationary solution of (29) is given by

$$c_k = -\frac{2\alpha}{k} \sum_p \frac{\cos p - 1}{p} c_p c_{k-p} , \quad (\text{B1})$$

where $c_{-k} = c_k^*$. In particular

$$c_1 = -\frac{2\alpha L^2}{4\pi^2} \left\{ \left[\cos \frac{2\pi}{L} - 1 \right] c_1 c_0 + \frac{1}{2} \left[\cos \frac{4\pi}{L} - 1 \right] c_2 c_{-1} - \left[\cos \frac{2\pi}{L} - 1 \right] c_{-1} c_2 + \dots \right\} \quad (\text{B2})$$

$$c_2 = -\frac{\alpha L^2}{4\pi^2} \left\{ \left[\cos \frac{2\pi}{L} - 1 \right] c_1 c_1 + \frac{1}{2} \left[\cos \frac{4\pi}{L} - 1 \right] c_2 c_0 + \dots \right\} \quad (\text{B3})$$

Close to $\alpha = \alpha_c$ the main contribution comes from the unstable mode. Therefore, we expand the solution in terms of c_1 . This can be done self-consistently through the *ansatz* $c_k \propto c_1^k$. For the mode corresponding to $k = 4\pi/L$ we obtain

$$c_2 = -\frac{1}{1 + \frac{\alpha L^2}{4\pi^2} \frac{1}{2} \left[\cos \frac{4\pi}{L} - 1 \right] c_0} \frac{\alpha L^2}{4\pi^2} \left[\cos \frac{2\pi}{L} - 1 \right] c_1^2. \quad (\text{B4})$$

This leads in third order in c_1 to Eq. (34), i.e.,

$$F(\alpha)c_1 - G(\alpha)|c_1|^2 c_1 = 0, \quad (\text{B5})$$

with

$$F(\alpha) = 1 + \frac{2\alpha L^2}{4\pi^2} \left[\cos \frac{2\pi}{L} - 1 \right] c_0 \quad (\text{B6})$$

and

$$G(\alpha) = \frac{2\alpha L^2}{4\pi^2} \left\{ \frac{1}{2} \left[\cos \frac{4\pi}{L} - 1 \right] - \left[\cos \frac{2\pi}{L} - 1 \right] \right\} \frac{\frac{\alpha L^2}{4\pi^2} \left[\cos \frac{2\pi}{L} - 1 \right]}{1 + \frac{\alpha L^2}{4\pi^2} \frac{1}{2} \left[\cos \frac{4\pi}{L} - 1 \right] c_0}. \quad (\text{B7})$$

In lowest order in $\alpha - \alpha_c$ the stationary solution is thus given by

$$|c_1| = \frac{Lc_0}{2\pi} \sqrt{\frac{-2c_0}{\cos \frac{2\pi}{L}}} \left[1 - \cos \frac{2\pi}{L} \right] (\alpha - \alpha_c)^{1/2} + O((\alpha - \alpha_c)^{3/2}) \quad (\text{B8})$$

Choosing $c_1 = |c_1|$ we finally obtain for the second Fourier-coefficient

$$c_2 = -\frac{2L^2 c_0^2}{4\pi^2} \frac{1 - \cos \frac{2\pi}{L}}{\cos \frac{2\pi}{L}} (\alpha - \alpha_c) + O\left((\alpha - \alpha_c)^2\right). \quad (\text{B9})$$

2. Bundles of mixed orientation

We determine solitary waves near α_c , which are oscillating solutions that can be expressed as

$$c^\pm(x, t) = \sum c_{k,n}^\pm e^{ikx} e^{i\omega nt}. \quad (\text{B10})$$

Writing out the equations for $c_{k,n}^\pm$ we see that the expressions for $c_{k,k}^\pm$ do not depend on Fourier-coefficients $c_{k,n}^\pm$ with $k \neq n$ and we may thus search for solutions with $c_{k,n}^\pm = 0$ for $k \neq n$. Explicitly, the solutions thus found are of the form $c^\pm(x + \frac{\omega L}{2\pi}t)$ and are thus solitary waves. Abbreviating $c_{k,k}^\pm$ by c_k^\pm we arrive at the following equations:

$$\begin{aligned} i\omega c_1^+ &= -\frac{4\pi^2}{L^2} c_1^+ + 2\alpha \left\{ \left[1 - \cos \frac{2\pi}{L} \right] (c_1^+ c_0^+ - c_{-1}^+ c_2^+) + \frac{1}{2} \left[1 - \cos \frac{4\pi}{L} \right] c_{-1}^+ c_2^+ + \dots \right\} \\ &\quad + 2i\beta \left\{ \frac{2\pi}{L} c_0^- c_1^+ + \sin \frac{2\pi}{L} (c_1^- c_0^+ + c_{-1}^- c_2^+) + \frac{1}{2} \sin \frac{4\pi}{L} c_2^- c_{-1}^+ + \dots \right\} \end{aligned} \quad (\text{B11})$$

$$\begin{aligned} 2i\omega c_2^+ &= -\frac{16\pi^2}{L^2} c_2^+ + 4\alpha \left\{ \left[1 - \cos \frac{2\pi}{L} \right] c_1^+ c_1^+ + \frac{1}{2} \left[1 - \cos \frac{4\pi}{L} \right] c_2^+ c_0^+ + \dots \right\} \\ &\quad + 4i\beta \left\{ \frac{2\pi}{L} c_0^- c_2^+ + \sin \frac{2\pi}{L} c_1^- c_1^+ + \frac{1}{2} \sin \frac{4\pi}{L} c_2^- c_0^+ + \dots \right\} \end{aligned} \quad (\text{B12})$$

$$\begin{aligned} i\omega c_1^- &= -\frac{4\pi^2}{L^2} c_1^- + 2\alpha \left\{ \left[1 - \cos \frac{2\pi}{L} \right] (c_1^- c_0^- - c_{-1}^- c_2^-) + \frac{1}{2} \left[1 - \cos \frac{4\pi}{L} \right] c_{-1}^- c_2^- + \dots \right\} \\ &\quad - 2i\beta \left\{ \frac{2\pi}{L} c_0^+ c_1^- + \sin \frac{2\pi}{L} (c_1^+ c_0^- + c_{-1}^+ c_2^-) + \frac{1}{2} \sin \frac{4\pi}{L} c_2^+ c_{-1}^- + \dots \right\} \end{aligned} \quad (\text{B13})$$

$$\begin{aligned} 2i\omega c_2^- &= -\frac{16\pi^2}{L^2} c_2^- + 4\alpha \left\{ \left[1 - \cos \frac{2\pi}{L} \right] c_1^- c_1^- + \frac{1}{2} \left[1 - \cos \frac{4\pi}{L} \right] c_2^- c_0^- + \dots \right\} \\ &\quad - 4i\beta \left\{ \frac{2\pi}{L} c_0^+ c_2^- + \sin \frac{2\pi}{L} c_1^+ c_1^- + \frac{1}{2} \sin \frac{4\pi}{L} c_2^+ c_0^- + \dots \right\}. \end{aligned} \quad (\text{B14})$$

⋮

In the following we assume without loss of generality $c_0^+ > c_0^-$, such that we may expand the solution on the bifurcating branch in terms of c_1^+ . Expansion up to third order in c_1^+ will finally lead to a quadratic equation for the non-trivial solution

$$F(\alpha, \beta, \omega) - G(\alpha, \beta, \omega) |c_1^+|^2 = 0, \quad (\text{B15})$$

where ω is the frequency associated to the limit cycle. At the bifurcation point $\alpha = \alpha_c$ we have $F(\alpha_c, \beta, \omega_0) = 0$. In first order in $\alpha - \alpha_c$ we obtain for the frequency and the amplitude of c_1^+

$$\omega = \omega_0 + \omega_1(\alpha - \alpha_c) + \dots \quad (\text{B16})$$

$$|c_1^+|^2 = \frac{\partial_\alpha F(\alpha_c, \omega_0) + \omega_1 \partial_\omega F(\alpha_c, \omega_0)}{G(\alpha_c, \omega_0)} (\alpha - \alpha_c) + \dots \quad (\text{B17})$$

The right hand side of the last expression needs to be real and positive such that we obtain the condition

$$\text{Im} \frac{\partial_\alpha F(\alpha_c, \omega_0)}{G(\alpha_c, \omega_0)} = \omega_1 \text{Im} \frac{\partial_\omega F(\alpha_c, \omega_0)}{G(\alpha_c, \omega_0)}. \quad (\text{B18})$$

Furthermore, the sign of the prefactor of $\alpha - \alpha_c$ will determine if the bifurcation is super- oder sub-critical.

After a somewhat lengthy calculation we obtain for F and G in first order in β :

$$F = -\frac{4\pi^2}{L^2} + 2\alpha \left[1 - \cos \frac{2\pi}{L} \right] c_0^+ + i \left[\frac{4\pi}{L} \beta c_0^- - \omega \right] \quad (\text{B19})$$

and

$$G = 8\alpha^2 \frac{L^2}{4\pi^2} \left[1 - \cos \frac{2\pi}{L} \right] \left\{ \left[1 - \cos \frac{2\pi}{L} \right] - \frac{1}{2} \left[1 - \cos \frac{4\pi}{L} \right] \right\} \left\{ \frac{1}{A} - 2i \frac{\omega_1 - \frac{4\pi^2}{L} c_0^-}{A^2} \beta \right\} \quad (B20)$$

where in the last expression $A = 16\pi^2/L^2 - 2\alpha [1 - \cos \frac{4\pi}{L}] c_0^+$. The condition $F(\alpha_c, \omega_0) = 0$ leads to

$$\alpha_c = \frac{4\pi}{L^2} \frac{1}{2 [1 - \cos \frac{2\pi}{L}] c_0^+} \quad (B21)$$

$$\omega_0 = \frac{4\pi}{L} \beta c_0^- \quad (B22)$$

implying

$$\partial_\alpha F(\alpha_c, \omega_0) = \frac{2L^2}{4\pi^2} [1 - \cos 2\pi L] c_0^+ \quad (B23)$$

$$\partial_\omega F(\alpha_c, \omega_0) = -i \frac{L^2}{4\pi^2} \quad (B24)$$

$$G(\alpha_c, \omega_0) = -\frac{1}{c_0^{22}} \frac{\cos \frac{2\pi}{L}}{1 - \cos \frac{2\pi}{L}}. \quad (B25)$$

This in turn leads to $\omega_1 = 0$. Thus up to first order in β the bifurcation is supercritical and subcritical for the same system lengths as in the case $\beta = 0$. The velocity of propagation follows to be $v = \omega L / 2\pi = 2\beta c_0^-$ consistent with the result obtained in Section III B. Furthermore, the components c_1^+ and c_2^+ are given by the expressions (B8) and (B9) for c_1 and c_2 , respectively, which had been obtained for the bifurcating branch in the case $\beta = 0$. For the distribution of minus-filaments we find

$$c_1^- = -2i\beta \frac{\sin \frac{2\pi}{L} c_0^-}{\frac{4\pi^2}{L^2} - 2\alpha [1 - \cos \frac{2\pi}{L}] c_0^+} c_1^+ \quad (B26)$$

$$c_2^- = i\beta \frac{\sin \frac{2\pi}{L} [1 - \cos \frac{2\pi}{L}]^2 c_0^{+2} c_0^-}{\frac{16\pi^4}{L^4} \left\{ 1 - \frac{1}{2} [1 + \cos \frac{2\pi}{L}] \frac{c_0^+ + c_0^-}{c_0^+} + \frac{1}{4} [1 + \cos \frac{2\pi}{L}]^2 \frac{c_0^-}{c_0^+} \right\}} (\alpha - \alpha_c) + O((\alpha - \alpha_c)^2). \quad (B27)$$

Finally we show, that in first order in β this result is the same as obtained from the calculation in Sec. III B 2 if u_0^+ in Eq. (44) is given by the stationary solution of Eq. (34) obtained in third order in the unstable mode. First of all note that in first order in β the solution for c^+ equals the solution for $\beta = 0$, see the text after Eq. (B25). Equivalently, $u_1^+ = 0$, see Eq. (43). With respect to the distribution for the minus-filaments, in expression (B26) for c_1^- one recognizes immediately Eq. (44) with $k = 2\pi/L$ and $u_{0,1}^+$ given by Eq. (B8). Finally, substituting in Eq. (44) for $k = 4\pi/L$ the value of $u_{0,2}^+$ by the expression given in Eq. (B9) we obtain, after a simple rearrangement

of terms, expression (B27). Thus, for $\alpha \rightarrow \alpha_c$ and $\beta \rightarrow 0$ the two different expansions lead to the same result.

ACKNOWLEDGMENTS

We thank J. Prost, S. Camalet, and K. Sekimoto for stimulating discussions. K. K. acknowledges financial support by the Max-Planck-Gesellschaft through a Schrödinger fellowship as well as the kind hospitality of the Landau Institute for Theoretical Physics, Moscow.

[1] B. Alberts, A. Johnson, J. Lewis, M. Raff, K. Roberts, and P. Walter, *Molecular biology of the cell* (Garland, New York, 2002), 4th ed.

[2] D. Bray, *Cell movements* (Garland, New York, 2001), 2nd ed.

[3] T. Kreis and R. Vale, *Cytoskeletal and motor proteins* (Oxford University Press, New York, 1993).

[4] F. Amblard, A. C. Maggs, B. Yurke, A. N. Pargellis, and S. Leibler, *Phys. Rev. Lett.* **77**, 4470 (1996).

[5] F. C. MacKintosh and P. A. Janmey, *Curr. Opin. Solid State & Mat. Sci.* **2**, 350 (1997).

[6] D. C. Morse, *Macromolecules* **31**, 7030 (1998), *ibid.* **31**,

7044 (1998), *ibid.* **32**, 5934 (1999).

[7] K. Takiguchi, *J. Biochem.* **109**, 520 (1991).

[8] R. Urrutia, M. A. McNiven, J. P. Albanesi, D. B. Murphy, and B. Kachar, *Proc. Natl. Acad. Sci.* **88**, 6701 (1991).

[9] F. Nédélec, T. Surrey, A. C. Maggs, and S. Leibler, *Nature* **389**, 305 (1997).

[10] T. Surrey, M. B. Elowitz, P.-E. Wolf, F. Yang, F. Nédélec, K. Shokat, and S. Leibler, *Proc. Natl. Acad. Sci. USA* **95**, 4293 (1998).

[11] F. Nédélec and T. Surrey, *C. R. Acad. Sci. Paris, Série IV* **2**, 841 (2001).

[12] T. Surrey, F. Nédélec, S. Leibler, and E. Karsenti, *Science* **292**, 1167 (2001).

[13] A. A. Hyman and E. Karsenti, *Cell* **84**, 401 (1996).

[14] U. Euteneuer and M. Schliwa, *Nature* **310**, 58 (1984).

[15] A. B. Verkhovsky, T. M. Svitkina, and G. G. Borisy, *Curr. Biol.* **9**, 11 (1999).

[16] D. Humphrey, C. Duggan, D. Saha, D. Smith, and J. Käs, *Nature* **416**, 744 (2002).

[17] O. Thoumine and A. Ott, *MRS Bull.* **25**, 22 (1999).

[18] H. Nakazawa and K. Sekimoto, *J. Phys. Soc. Jpn.* **65**, 2404 (1996).

[19] K. Sekimoto and H. Nakazawa, in *Current topics in physics*, edited by Y. M. Cho, J. B. Hong, and C. N. Yang (World Scientific, Singapore, 1998), p. 394, physics/0004044.

[20] K. Kruse and F. Jülicher, *Phys. Rev. Lett.* **85**, 1778 (2000).

[21] K. Kruse, S. Camalet, and F. Jülicher, *Phys. Rev. Lett.* **87**, 138101 (2001).

[22] S. Camalet, F. Jülicher, and J. Prost, *Phys. Rev. Lett.* **82**, 1590 (1999).

[23] S. Camalet and F. Jülicher, *New J. Phys.* **2**, 24 (2000).

[24] B. Bassetti, M. C. Lagomarsino, and P. Jona, *Eur. Phys. J. B* **15**, 483 (2000).

[25] H. Y. Lee and M. Kardar, *Phys. Rev. E* **64**, 056113 (2001).

[26] T. B. Liverpool, A. C. Maggs, and A. Ajdari, *Phys. Rev. Lett.* **86**, 4171 (2001).

[27] F. Jülicher, A. Ajdari, and J. Prost, *Rev. Mod. Phys.* **69**, 1269 (1997).

[28] A. Ishijima, H. Kojima, H. Higuchi, Y. Harada, T. Funatsu, and T. Yanagida, *Biophys. J.* **70**, 383 (1996).

[29] F. Nédélec, T. Surrey, and A. C. Maggs, *Phys. Rev. Lett.* **86**, 3192 (2001).

[30] J. Howard, *Nature* **389**, 561 (1997).

[31] K. Kruse and F. Jülicher, to be published.

[32] K. Kruse and K. Sekimoto (2002), *Phys. Rev. E*, in press.